Enhancement of Quantum Sensing in a Cavity Optomechanical System around Quantum Critical Point

Shao-Bo Tang, ¹ Hao Qin, ¹ Bing-Bing Liu, ¹ D.-Y. Wang, ¹, * Kaifeng Cui, ¹ S.-L. Su, ¹, [†] L.-L. Yan, ¹, [‡] and Gang Chen ¹ School of Physics, Zhengzhou University, Zhengzhou 450001, China (Dated: October 11, 2024)

The precision of quantum sensing could be improved by exploiting quantum phase transitions, where the physical quantity tends to diverge when the system is approaching the quantum critical point. This critical enhancement phenomenon has been applied to the quantum Rabi model in a dynamic framework, showing a promising sensing enhancement without the complex initial state preparation. In this work, we find a quantum phase transition in the coupling cavity-mechanical oscillator system when the coupling strength crosses a critical point, determined by the effective detuning of cavity and frequency of mechanical mode. By utilizing this critical phenomenon, we obtain a prominent enhancement of quantum sensing, such as the position and momentum of the mechanical oscillator. This result provides an alternative method to enhance the quantum sensing of some physical quantities, such as mass, charge, and weak force, in a large mass system.

I. INTRODUCTION

To check new theories, it always needs to improve the measurement precision, together with promoting the development of new technologies, among which the superprecision measurement has been a heavily researched area [1–4]. Quantum sensing, as one advancing technology to carry out the super-precision measurement, can significantly improve measurement precision by exploiting quantum phenomena such as quantum superposition, entanglement, and criticality [5–7]. The essence of measurement precision is the relevant parameters' susceptibility. By utilizing the high sensibility characteristic to minute changes in physical parameters around the quantum critical point, the measurement precision can be greatly enhanced [8–11].

The specific quantum sensing in the laboratory is divided into four steps: 1) Initial state preparation [12–15]; 2) Dynamic process [4, 16, 17]; 3) Final state measurement; 4) Parameter estimation [18, 19]. The preparation of the initial state is a crucial step among these four steps because its quality directly determines the precision of parameter estimation. Actually, one effective but challenging method to enhance the quantum sensing is to prepare a ground state close to the critical points. Recently, some works demonstrate the feasibility that a high precision can be achieved through the relaxed initial state preparation by utilizing quantum phase transition (QPT) [10, 11]. QPT shows a divergence when the system, such as the Dicke model [20], crosses from the normal phase to the superradiance phase in the thermodynamic limit. Further researches show that the QPT can also occur in a finite component system [21-24], such as the Rabi model [25], where the QPT appears when the atomic transition frequency is much greater than optical field frequency [26, 27]. Therefore, the QPT in the Rabi model [10] can

be used to enhance the quantum sensing for the precision measurement with a relaxed initial state.

A typical cavity optomechanical system (COMS), consisting of a mechanical oscillator, optical cavity, and driving laser [28–30], can be used as a powerful tool for exploring the precision measurement [31], quantum sensing [8], and quantum information [32] due to its macroscopic quantum properties. Recently, some researches have pay attention to the phase transition of COMS to reinforce the precision measurement [33, 34]. However, limited by the cavity decay rate and coupling strength, it is still a challenge for realizing various quantum states of COMS [35–37]. With the natural advantages of COMS in quantum sensing, how to relax the requirement for state preparation and further enhance quantum sensing in this system would make sense for the ultra-precision measurements.

In this work, we study the enhancement of quantum sensing by exploiting the QPT in a typical COMS. We find a divergent feature of the quantum Fisher information (QFI) around the quantum critical point, and then elaborate that the precision of measurement based on QPT can be close to the quantum Cramér-Rao bound [38–40]. Moreover, the QFI does not require specific initial state preparation, thus simplifying the experimental requirements, and the adjustable drive laser in the COMS also provides a more convenient method to satisfy the frequency relationship than the standard Rabi model. Furthermore, the parameter of QPT is proportional to the optomechanical coupling strength, which means that phase transition could be obtained by turning the drive laser power. Since mechanical oscillators can be regarded as a bridge coupled to various physical systems and are suitable for detecting quantities such as mass, charge, and weak force [41–43], our work paves the way for high-sensitivity measurement by using a mechanical oscillator around the quantum critical point.

The rest of this paper is organized as follows: In Sec. II, we provide the Hamiltonian of COMS in the rotating frame and then linearize it to discuss the dynamic phase transition around the quantum critical point. In Sec. III, we demonstrate the calculation process of the QFI for

^{*} dywang@zzu.edu.cn

[†] slsu@zzu.edu.cn

[‡] llyan@zzu.edu.cn

the parameter-dependent Hamiltonian. Sec. IV shows the results of quadrature measurements by homodyne detection, and analyzes the error introduced by the finite frequency ratio with different initial states. Finally, we briefly discuss the experimental feasibility in Sec. V and give a conclusion in Sec. VI.

II. QUANTUM PHASE TRANSITION IN COMS

A typical COMS is shown in Fig. 1, where the system consists of a single-mode field and a nanomechanical oscillator [44, 45], and its Hamiltonian is $(\hbar = 1)$

$$H = \omega_c a^{\dagger} a + \omega_m b^{\dagger} b - g a^{\dagger} a \left(b^{\dagger} + b \right) + i \varepsilon_l \left(e^{-i\omega_l t} a^{\dagger} - e^{i\omega_l t} a \right).$$
 (1)

The first and second terms represent the free energy of cavity field and nanowire oscillator, the third term is the optomechanical coupling term with the coupling strength g, and the last term is regarded as the driving term with the driving amplitude ϵ_l . Performing the rotation transformation under $U = e^{-i\omega_l t a^{\dagger} a}$, the Hamiltonian is simplified as

$$H' = \delta a^{\dagger} a + \omega_m b^{\dagger} b - g a^{\dagger} a \left(b^{\dagger} + b \right) + i \varepsilon_l \left(a^{\dagger} - a \right) \quad (2)$$

where $\delta = \omega_c - \omega_l$ is the detuning between the cavity field frequency and the driving laser frequency.

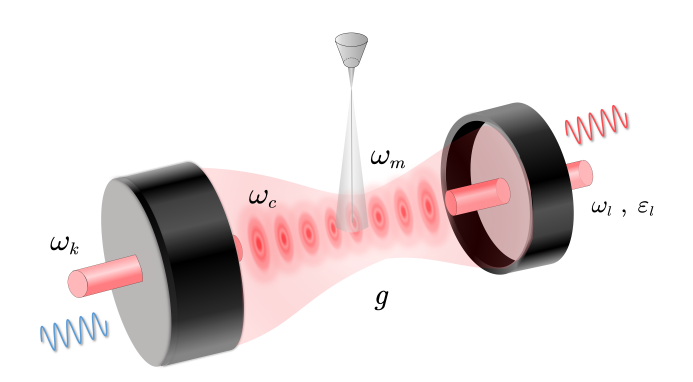


FIG. 1. Cavity optomechanical system consists of an optical cavity with frequency ω_c (expressed by operators a and a^{\dagger}), a mechanical oscillator with frequency ω_m (expressed by operators b and b^{\dagger}) and g is the optomechanical coupling strength. ω_k is the frequency of cooling laser and ω_l is the frequency of drive laser (ε_l is amplitude).

Considering the influence of environmental thermal noise on COMS, the motion equations of system are given by

$$\dot{a} = \left(-i\delta - \frac{\gamma_c}{2}\right)a + iga\left(b^{\dagger} + b\right) + \varepsilon_l + \sqrt{\gamma_c}a_{in},$$

$$\dot{b} = \left(-i\omega_m - \frac{\gamma_m}{2}\right)b + iga^{\dagger}a + \sqrt{\gamma_m}b_{in},$$
(3)

where a_{in} and b_{in} are noise operators of optical mode and mechanical mode, respectively, and $\gamma_{c,m}$ are the dissipation of system corresponding to the operators of a_{in} and b_{in} .

Replace the operators by their average values plus fluctuations driven by strong laser, i.e., $a \to \langle a \rangle + \delta a$, $b \to \langle b \rangle + \delta b$ where $\langle a \rangle$ and $\langle b \rangle$. In the following, we replace the fluctuation δa and δb by a and b for convenience. Then, the evolution equations for the mean amplitudes can be obtained as

$$\langle \dot{a} \rangle = \left[i \left(2g \langle b \rangle - \delta \right) - \frac{\gamma_c}{2} \right] \langle a \rangle + \varepsilon_l,$$

$$\langle \dot{b} \rangle = \left(-i\omega_m - \frac{\gamma_m}{2} \right) \langle b \rangle + ig \langle a \rangle^2,$$
(4)

and the evolution equations of fluctuation operators are given as

$$\dot{a} = \left[i\left(2g\langle b\rangle - \delta\right) - \frac{\gamma_c}{2}\right]a + ig\langle a\rangle\left(b^{\dagger} + b\right) + \sqrt{\gamma_c}a_{in},$$

$$\dot{b} = \left(-i\omega_m - \frac{\gamma_m}{2}\right)b + ig\langle a\rangle\left(a^{\dagger} + a\right) + \sqrt{\gamma_m}b_{in}.$$

Under a strong laser driving, the coherent amplitudes reach their steady state with

$$\langle a \rangle = \frac{\varepsilon_l}{\gamma_c/2 - i(2g\langle b \rangle - \delta)}, \quad \langle b \rangle = \frac{ig\langle a \rangle^2}{i\omega_m + \gamma_m/2}.$$
 (6)

At this time, the Hamiltonian corresponding to these Langevin equations of fluctuation operators is

$$H_L = \Delta a^{\dagger} a + \omega_m b^{\dagger} b - G \left(a^{\dagger} + a \right) \left(b^{\dagger} + b \right), \quad (7)$$

where the effective detuning between the cavity field frequency and the driving laser frequency is $\Delta = \delta - 2g\langle b \rangle$, and the enhanced effective optomechanical coupling strength $G = g\langle a \rangle$ [46, 47].

By utilizing the Schriffer-Wolff (SW) transformation [48, 49] to eliminate the off-diagonal part in H_L , we obtain an approximated appropriate unitary transformation e^S . The generator $S = G(b^{\dagger} + b)(a^{\dagger} - a)/\omega_m$ is anti-Hermitian and block-off-diagonal under the condition of $\eta = \Delta/\omega_m \gg 1$, which makes the transformed Hamiltonian $e^{S^{\dagger}}H_Le^S$ free of the coupling terms between cavity field and nanomechanical oscillator. Consequently, projecting onto $|n_a = 0\rangle$, we obtain the effective Hamiltonian as

$$\mathcal{H}_L = \omega_m b^{\dagger} b - \frac{\lambda^2 \omega_m}{4} (b^{\dagger} + b)^2, \tag{8}$$

with $\lambda = 2G/\sqrt{\Delta\omega_m}$. Eq. (8) can be diagonalized by the squeezing operator $S(r_{\rm np}) = \exp[r_{np}(b^{\dagger 2} - b^2)/2]$ with squeezing amplitude $r_{\rm np} = \ln(1 - \lambda^2)/4$, i.e., $\mathcal{H}'_L = S^{\dagger}(r_{\rm np})\mathcal{H}_LS(r_{\rm np}) = \epsilon_{\rm np}b^{\dagger}b + E_{\rm np}$ where $E_{\rm np} = (\epsilon_{np} - \omega_m)/2$ is ground state energy and $\epsilon_{np} = \omega_m\sqrt{1 - \lambda^2}$ is the excitation frequency [27]. Generally, the excitation frequency $\epsilon_{\rm np}$ is required to be real, which indicates $\lambda < 1$, i.e., $G < G_c = \sqrt{\Delta\omega_m}/2$. Hence, G_c is the critical point, and $G < G_c$ is the normal phase while the COMS enters the superradiant phase if $G > G_c$.

III. QFI OF CRITICAL QUANTUM DYNAMICS

The performance of quantum sensing is determined by the sensitivity of two neighboring states, characterized by QFI. Consider a parameter (ξ)-dependent Hamiltonian $H_{\xi} = H_0 + \xi H_1$ and the system is initially prepared in $|\Psi_0\rangle$. After the dynamic evolution $U_{\xi} = \exp(-iH_{\xi}t)$, the state of the system becomes $\rho_{\xi} = U_{\xi}^{\dagger}|\Psi_0\rangle\langle\Psi_0|U_{\xi}$. The QFI, which characterizes the sensitivity between ρ_0 and $\rho_{\xi+\mathrm{d}\xi}$ with d ξ denoting the infinitesimal change of ξ , is $I_{\xi} = 4\mathrm{Var}[h_{\xi}]_{|\Psi_0\rangle}$, where $\mathrm{Var}[\dots]_{|\Psi_0\rangle}$ represents the variance corresponding to the initial state, and $h_{\xi} = iU_{\xi}^{\dagger} (\partial_{\xi}U_{\xi})$ is the generator of parameter translation with respect to ξ [50, 51]. Therefore, the key mission to calculating QFI is h_{ξ} .

By the integral formula for the derivative of an operator exponential $\partial_x e^{-yH(x)} = -\int_0^y e^{-(y-u)H(x)} \partial_x H(x) e^{-uH(x)} du$ [52], we obtain the integral form of h_ξ is

$$h_{\xi} = \int_{0}^{t} e^{iH_{\xi}u} H_{1} e^{-iH_{\xi}u} du = \int_{0}^{t} \sum_{n=0}^{\infty} \frac{(iu)^{n}}{n!} \left[H_{\xi}^{(n)}, H_{1} \right] du$$
$$= -i \sum_{n=0}^{\infty} \frac{(it)^{n+1}}{(n+1)!} \left[H_{\xi}^{(n)}, H_{1} \right]. \tag{9}$$

To get the result of Eq. (9), we first construct the Hamiltonian H_{ξ} satisfying the following reciprocal relationship

$$[H_{\xi}, \Gamma] = \sqrt{\Lambda}\Gamma, \tag{10}$$

where Λ is dependent on the parameter λ , H_{ξ} can be regarded as superoperator acting on Γ , and $\Gamma = i\sqrt{\Lambda}C - D$ with $C = -i\left[H_0, H_1\right]$ and $D = -\left[H_{\xi}, \left[H_0, H_1\right]\right]$. Then, making the system satisfy the following commutation rules

$$\begin{split} \left[H_{\xi}^{(2n+1)}, H_1\right] &= i\Lambda^n C, \\ \left[H_{\xi}^{(2n+2)}, H_1\right] &= -\Lambda^n D, \quad (n \in \mathbb{N}), \end{split} \tag{11}$$

Eq. (9) can be further simplified to

$$h_{\xi} = H_1 t + \frac{\cos(\sqrt{\Lambda}t) - 1}{\Lambda} C - \frac{\sin(\sqrt{\Lambda}t) - \sqrt{\Lambda}t}{\Lambda^{\frac{3}{2}}} D, \quad (12)$$

which shows that h_{ξ} tends to divergent as $\Lambda \to 0$ in the condition of $\sqrt{\Lambda} \simeq \mathcal{O}(1)$, demonstrating a critical effect. Taking Eq. (12) into $I_{\xi} = 4 \mathrm{Var}[h_{\xi}]_{|\Psi_0\rangle}$ and in the limit $\lambda \to 1$, we finally obtain the QFI as (see Appendix A for details) [10],

$$I_{\xi} \simeq 4 \frac{\left[\sin(\sqrt{\Lambda}t) - \sqrt{\Lambda}t\right]^2}{\Lambda^3} \text{Var}\left[D\right]_{|\Psi_0\rangle}.$$
 (13)

 I_{ξ} diverges as Λ^{-3} under the conditions of $\sqrt{\Lambda} \simeq \mathcal{O}(1)$ and $\mathrm{Var}\,[D]_{|\Psi_0\rangle} \neq 0$ for the pure initial state $|\Psi_0\rangle$.

Assuming that Eq. (8) satisfies the relation in Eq. (10), we define the quadrature operators as $X = (b^{\dagger} + b)/\sqrt{2}$ and $P = i(b^{\dagger} - b)/\sqrt{2}$ before calculating the QFI of \mathcal{H}_L . Then, \mathcal{H}_L can be rewritten as

$$\mathcal{H}'_{L} = \frac{\omega_{m}}{2} \left[P^{2} + \left(1 - \lambda^{2} \right) X^{2} \right]. \tag{14}$$

Comparing the form of Eq. (14) with $H_{\xi} = H_0 + \xi H_1$, we choose $H_0 = \omega_m P^2/2$ and $H_1 = \omega_m X^2/2$. Utilizing the method of Eq. (10), we get $\Lambda = 4\omega_m^2 \xi$ with the parameter $\xi = 1 - \lambda^2$ and

$$C = \frac{\omega_m^2 (XP + PX)}{2},$$

$$D = \omega_m^3 \left[P^2 - (1 - \lambda^2) X^2 \right].$$
(15)

At this time we can obtain the QFI of \mathcal{H}_L for the measurement of the parameter λ as

$$I_{\lambda}(t) = (\partial_{\lambda}\xi)^{2}I_{\eta}(t)$$

$$\simeq 16\lambda^{2} \frac{\left[\sin(\sqrt{\Lambda}\omega_{m}t) - \sqrt{\Lambda}\omega_{m}t\right]^{2}}{\Lambda^{3}} \operatorname{Var}\left[P^{2}\right]_{|\varphi\rangle},$$
(16)

where the parameter $\Lambda = 4(1-\lambda^2) \ll 1$ and $\mathrm{Var}\left[D\right]_{|\Psi_0\rangle} \simeq \omega_m^6 \mathrm{Var}\left[P^2\right]_{|\Psi_0\rangle}$ as $\xi \to 0$ for the initial state $|\Psi_0\rangle$. It also shows that $I_\lambda(t)$ is divergent as $\xi \to 0$ (i.e., $\Lambda \to 0$), thus, the measurement precision can be enhanced around the quantum critical point. Next, We will introduce a feasible high-precision measurement method based on the above results.

IV. THE MEASUREMENT PRECISION OF SYSTEM

A. Superposition State as the Initial State

We prepare the system in a product state $|\Psi_0\rangle = |n_a = 0\rangle \otimes |\varphi\rangle_m$ with the state of mechanical field mode $|\varphi\rangle_m = (|0\rangle + i|1\rangle)/\sqrt{2}$. After an evolution for time t, governed by the effective Hamiltonian of COMS in Eq. (14), the motion equations of quadrature operators X, in the Heisenberg picture, can be obtained as (see Appendix B for details)

$$\langle X \rangle_t = \sqrt{2} \Lambda^{-\frac{1}{2}} \sin\left(\sqrt{\Lambda}\omega_m t/2\right),$$

$$(\Delta X)^2 = 1 + (2\lambda^2 - 1) \Lambda^{-1} \left[1 - \cos\left(\sqrt{\Lambda}\omega_m t\right)\right].$$
 (17)

As shown in Fig. 2(a), $\langle X \rangle_t$ as a function of λ after an evolution time $\tau = \pi / \left[\omega_m \left(\sqrt{1 - \lambda_0^2} \right) \right]$ is sensible around working point λ_0 and the derivative of $\langle X \rangle_t$ tends to diverge as $\lambda_0 \to 1$.

Defining a function $\mathcal{I}_{\lambda}(t) = (\partial_{\lambda}\langle X\rangle_{t})^{2}/(\Delta X)^{2}$, the estimation error is then given by $\mathcal{I}_{\lambda}^{-1}(t)$. When $\mathcal{I}_{\lambda}(t) = I_{\lambda}(t)$, the estimation error reaches the quantum Cramér-Rao bound (i.e., reciprocal of QFI). As shown in Fig. 2(b), the periodic peaks of $\mathcal{I}_{\lambda}(t)$ are obtained at the evolution time $\tau_{n} = 2n\pi/\sqrt{\Lambda}\omega_{m}$ with the peak value $\mathcal{I}_{\lambda}(\tau_{n}) = 32\lambda^{2}\pi^{2}n^{2}\Lambda^{-3}$, which is the same order with the corresponding QFI $I_{\lambda}(\tau_{n}) \simeq 64\lambda^{2}\pi^{2}n^{2}\Lambda^{-3}\mathrm{Var}\left[P^{2}\right]_{|\varphi\rangle_{m}}$ according to Eq. (16), which can been seen from the inset of Fig. 2(b). Besides, we can also find that both the values of $I_{\lambda}(\tau_{n})$ and $\mathcal{I}_{\lambda}(\tau_{n})$ become larger as $\lambda \to 1$

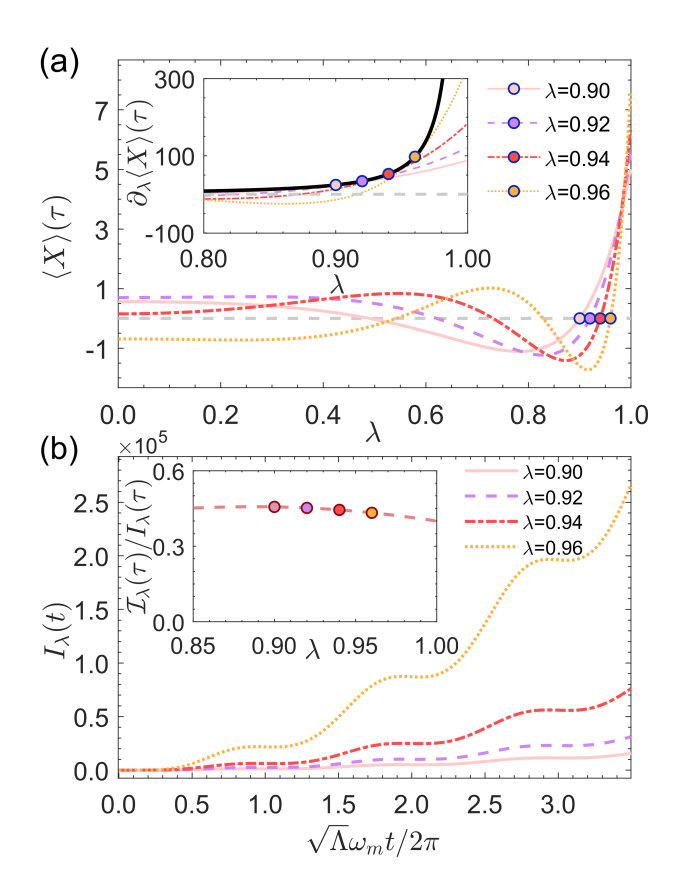


FIG. 2. Quantum sensing by homodyne detection of the mechanical field. (a) Quadrature $\langle X \rangle_{\tau}$ as a function of λ after an evolution time $\tau = 2\pi/(\omega_m \sqrt{\Lambda_{\lambda_0}})$ with $\Lambda_{\lambda_0} = 4(1-\lambda_0)^2$. The filled circles represent $\lambda = \lambda_0$. Inset: This figure shows the susceptibilty $\partial_{\lambda} \langle X \rangle_{\tau}$ as a function of λ after the same evolution time τ . The black solid line with filled circles illustrate the graphics of $\partial_{\lambda} \langle X \rangle_{\tau}$ at $\lambda_0 = \lambda$. (b) The QFI I_{λ} as a function of evolution time t. Inset: the ratio between $\mathcal{I}_{\lambda}(\tau)$ and $I_{\lambda}(\tau)$ after an evolution time $\tau = 2\pi/(\omega_m \sqrt{\Lambda})$.

and increase of τ_n , which means that the bound of precision is higher (the larger $I_{\lambda}(\tau_n)$) and the measurement can achieve with a higher precision (the larger $\mathcal{I}_{\lambda}(\tau)$). It is worth noting that these results do not require particular initial states of mechanical field mode. Thus, the quantum sensing can be realized without a complex state preparation by encoding the physical parameter in the optomechanical cavity.

B. The Influence of Finite Frequency Ratio

The above discussion is based on the thermodynamic limit condition $\eta = \Delta/\omega_m \to \infty$, which is just an ideal situation and neglects the higher order terms of the Hamiltonian of COMS after the SW transformation, however, it only can achieve finite value η in the actual condition. Therefore, the purpose of this section is to explore the influence of higher-order terms in the SW transformation of the COMS Hamiltonian. Correcting $S = G(b^{\dagger} + b)(a^{\dagger} - a)/\omega_m$ into \tilde{S} , we can get the cor-

rected Hamiltonian \tilde{H}_L (See Eq. (C6) and Eq. (C7) in Appendix C), which results in a correction on Eq. (17), i.e., $\langle \tilde{X} \rangle_t = \langle X \rangle_t + \langle X \rangle_c$ and $(\Delta \tilde{X})^2 = (\Delta X)^2 + (\Delta X_c)^2$. Hence, we can obtain the dynamics of the quadrature in the condition of finite frequency ratio as

$$\langle \tilde{X} \rangle_{t} = \langle \Psi | e^{iH_{L}t} X e^{-iH_{L}t} | \Psi \rangle$$

$$= \langle \Psi | e^{\tilde{S}} e^{i\mathcal{H}_{L}t} e^{-\tilde{S}} X e^{\tilde{S}} e^{-i\mathcal{H}_{L}t} e^{-\tilde{S}} | \Psi \rangle$$

$$= \langle \Psi | \left[1 + \mathcal{O}(\eta^{-\frac{1}{2}}) \right] e^{i\mathcal{H}_{L}t} X \left[\left[1 + \mathcal{O}(\eta^{-1}) \right] \right]$$

$$e^{-i\mathcal{H}_{L}t} \left[\left[1 + \mathcal{O}(\eta^{\frac{1}{2}}) \right] | \Psi \rangle, \tag{18}$$

with $|\Psi\rangle = |\Psi_0\rangle$. The leading term $\langle \Psi|e^{i\tilde{H}_Lt}Xe^{-i\tilde{H}_Lt}|\Psi\rangle$ is equal to $\langle X\rangle_t$ and the dominant contribution to correction is on the order of $\eta^{-1/2}\langle X\rangle_t \sim (\eta\Lambda)^{-1/2}$.

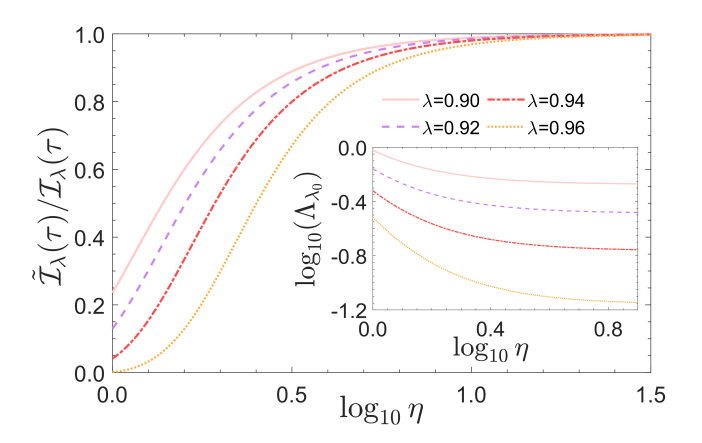


FIG. 3. The ratio between $\tilde{\mathcal{I}}_{\lambda}(\tau)$ and $\mathcal{I}_{\lambda}(\tau)$ for finite frequency ratio η in the condition of $\eta \to \infty$ after an evolution time $\tau = 2\pi/(\omega_m\sqrt{\Lambda})$. Inset: the parameter $\Lambda_{\lambda_0} = 4(1-\lambda_0)^2$ corresponds to the working point λ_0 at which $\tilde{\mathcal{I}}_{\lambda}(\tau)$ achieves its local maximums. These solid curves satisfy the relation $\log_{10}[\Lambda_{\lambda_0}] = \log_{10}[4(1-\lambda)^2 + \lambda^4\eta^{-2}]/3$.

In order to evaluate the influence of the transformed Hamiltonian \tilde{H}_L , where the major influence is from $\lambda^2 \eta^{-1}$, we recalculate the Heisenberg equations of quadrature and obtain the correction $\langle X \rangle_c \sim \eta^{-2} \Lambda^{-3/2}$, which is more important than the order of $(\eta \Lambda)^{-1/2}$ derived from SW transformation. Similarly, the correction to the variance of the quadrature $(\Delta \tilde{X})^2$ can be obtain as $(\Delta X_c)^2 \sim \eta^{-2} \Lambda^{-2}$. Thus, the analysis in the above section will remain valid in the condition of $\Lambda \gg \eta^{-1}$ and correction terms can be negligible compared with $\Delta X(\tau_n) = 1$ when $t = \tau_n$. As shown in Fig. 3, the performance of our solutions can be sustained when the condition is satisfied.

C. Measurement Precision of Coherent State

The above calculations are based on the mechanical superposition state in Sec. IV, which is not easy prepared in most mechanical systems. Here, we discuss the performance based on a coherence state around the critical point for more application. Firstly, we prepare a product state $\Psi_0 = |n_a = 0\rangle \otimes |\alpha\rangle$ with $|\alpha\rangle$ denoting the coherence state of mechanical oscillator. Then, the equations of quadrature operators X can be obtained in the Heisenberg picture with its mean value and variance given by

$$\langle X^{(\alpha)} \rangle (t) = \sqrt{2} \Lambda^{-\frac{1}{2}} \operatorname{Im} (\alpha) \sin \left(\sqrt{\Lambda} \omega_m t / 2 \right) + \sqrt{2} \operatorname{Re} (\alpha) \cos \left(\sqrt{\Lambda} \omega_m t / 2 \right),$$

$$\left(\Delta X^{(\alpha)} \right)^2 (t) = \frac{1}{4} + \left(1 - \lambda^2 \right) \Lambda^{-1} \cos(\sqrt{\Lambda} \omega t),$$
(19)

with $\operatorname{Im}(\alpha)$ and $\operatorname{Re}(\alpha)$ denoting the real part and imaginary part of α , respectively. Thus, we have the function $\mathcal{I}_{\lambda}^{(\alpha)}(\tau_n) = (\partial_{\lambda}\langle X^{(\alpha)}\rangle_{\tau_n})^2/(\Delta X_{\tau_n}^{(\alpha)})^2 = 64\pi^2\lambda^2\Delta^{-3}\operatorname{Im}^2(\alpha)$ at evolution time $\tau_n = 2n\pi/\sqrt{\Lambda}\omega_m$ with τ_n still denoting the positions of peak values of $\mathcal{I}_{\lambda}^{(\alpha)}(\tau_n)$. As expected, it keep the same order of $I_{\lambda}^{(\alpha)}(\tau_n) \simeq 64\lambda^2\pi^2n^2\Lambda^{-3}\operatorname{Var}\left[P^2\right]_{|\varphi\rangle_m}$, which means that the coherence state can also achieve the super-precision.

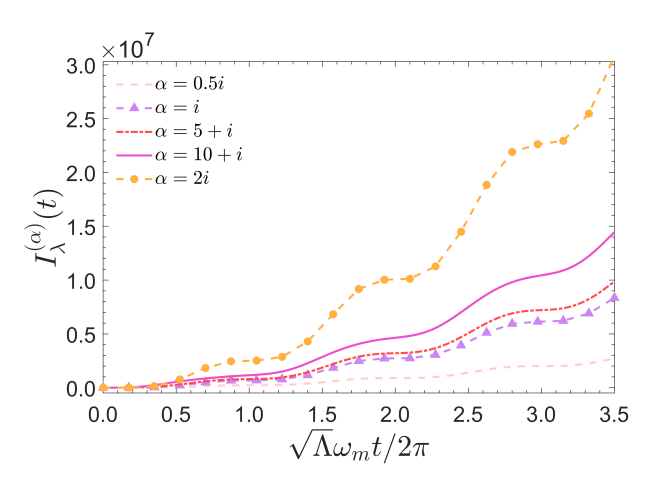


FIG. 4. The QFI $I_{\lambda}^{(\alpha)}$ as a function of evolution time t with different α , where we choose $\lambda=0.98$.

Due to the similar critical behaviour as the superposition state, we assign λ to 0.98 to analyze the role of α . As shown in Fig. 4, the QFI of the coherence state is affected by both $\mathrm{Re}(\alpha)$ and $\mathrm{Im}(\alpha)$. In addition, $\mathrm{Im}(\alpha)$ has a greater influence on $I_{\lambda}^{(\alpha)}$ and totally controls the value of $\mathcal{I}_{\lambda}^{(\alpha)}$ which can be reflected in Fig. 5. When $\mathrm{Im}(\alpha)$ takes a larger value, the estimation error is closer to Cramér-Rao bound. However, the ratio $\mathcal{I}_{\lambda}^{(\alpha)}/I_{\lambda}^{(\alpha)}$ becomes smaller as $\mathrm{Re}(\alpha)$ increases which means that the real part of initial state will damage the sensitivity of quantum sensing. The reason is that the function $\mathcal{I}_{\lambda}^{(\alpha)}$ remains constant while $I_{\lambda}^{(\alpha)}$ becomes larger, i.e., Cramér-Rao bound becomes lower. Therefore, the enhancement of quantum sensing can be realized without harsh state preparation in COMS and it would own more superiority for the coherent state with a larger imaginary part.

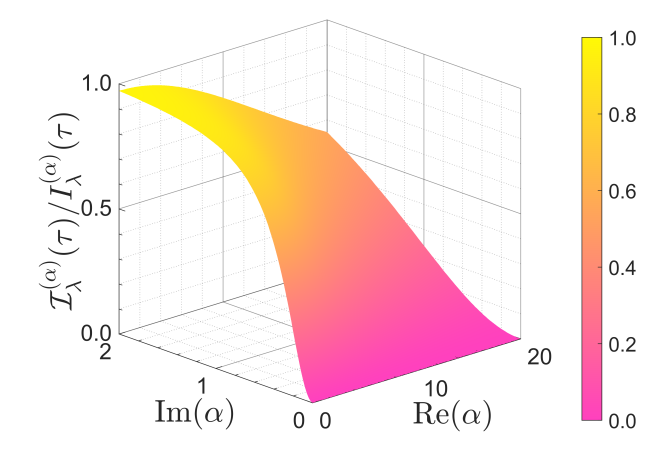


FIG. 5. The ratio between $\mathcal{I}_{\lambda}^{(\alpha)}(\tau)$ and $I^{(\alpha)}\lambda(\tau)$ with $\lambda=0.98$ after an evolution time $\tau=\pi/(\omega_m\sqrt{1-\lambda^2})$. Re(α) is negatively related to the ratio and Im(α) is positively related to the ratio.

Next, we are curious about the performance of $\mathcal{I}_{\lambda}^{(\alpha)}$ with finite frequency. The major influence is still discussed by the motion equation of quadrature, $\langle X \rangle_c^{(\alpha)} \sim \eta^{-2} \Lambda^{-3/2}$ and $(\Delta X_c)^2 \sim \eta^{-2} \Lambda^{-2}$. When $\Lambda \gg \sqrt{2} \eta^{-1}$, the correction terms can be neglected. After calculation, we find that the ratio $\tilde{\mathcal{I}}_{\lambda}^{(\alpha)}/\mathcal{I}_{\lambda}^{(\alpha)}$ will not be affected by the imaginary part $\text{Im}(\alpha)$ of coherent state. However, as shown in Fig. 6, the system requires a larger frequency ratio to reduce the impact of correction terms when $\text{Re}(\alpha)$ increases.

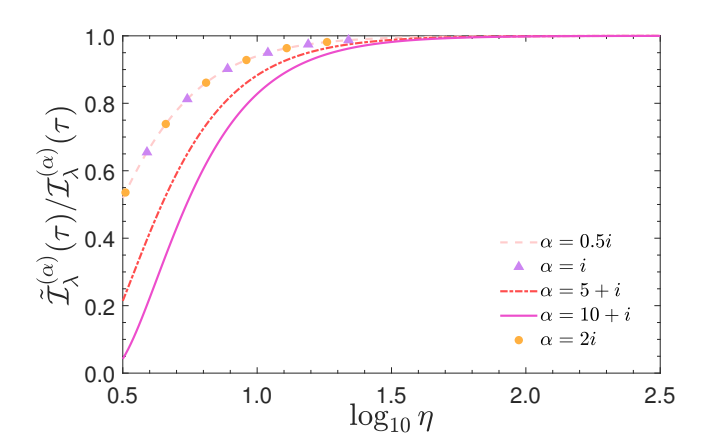


FIG. 6. The ratio between $\tilde{\mathcal{I}}_{\lambda}^{(\alpha)}(\tau)$ and $\mathcal{I}_{\lambda}^{(\alpha)}(\tau)$ for the finite frequency ratio η in the condition $\eta \to \infty$ after an evolution time $\tau = \pi/(\omega_m \sqrt{1-\lambda^2})$ ($\lambda = 0.98$). Dash line, triangle and circle are overlapped together when α takes a pure imaginary number.

V. EXPERIMENTAL FEASIBILITY

The dynamic framework in this article requires less fluctuation of phonon number so that the QPT phenomenon of mechanical oscillator quantum fluctuation

is evident. For this reason, we need to manipulate a strong laser to cool the nanomechanical oscillator into its ground state by some cooling methods, such as the sideband cooling [53], optical feedback cooling [54], and radiation pressure cooling [55]. We insert a silicon carbide nanowire into a high-finesse fiber microcavity in static, insulated, and cryogenic (T = 15 mK) vacuum, where its quality factor is about 10⁶ and cavity length is 200 μ m [45]. The employed nanowire with effective masses around M = 48 pg, diameter d = 130 nm, and length $L = 10 \ \mu \text{m}$ can vibrate with a frequency obout $\omega_m/2\pi = 10.56$ MHz. To cool the nanomechanical oscillator, we can utilize an additional pump field with laser frequency ω_k , satisfying the red-sideband resonance condition $\omega_c - \omega_k \sim \omega_m$. Moreover, the ground-state cooling of the nanomechanical oscillator has been realized experimentally in various systems [44, 53, 56, 57]. The huge frequency ratio $(\omega_c - \omega_l)/\omega_m$ needed in this proposal can be easily obtained by adjusting the frequency of driving laser ω_l , where the frequency of driving laser and microcavity is in the optical range and much greater than the oscillator frequency. The optomechanical coupling strength is inherently tunable via the driving power, which further adjusts the parameter λ near the quantum critical point. In addition, we need to prepare the nanomechanical oscillator into a superposition state or a coherence state. The preparation of these states has already been reported in the trapped-ion oscillator system [58, 59]. In macroscopic ensemble, the coherent state has been realized in Kerr parametric oscillator [60], and the superposition state has been relatively well established in theory [61–63]. Therefore, this dynamic framework is expected to be experimentally feasible and applied to super-precision measurement.

VI. CONCLUSION

In conclusion, we have investigated the QPT of COMS and explored the quantum sensing around the quantum critical point without the specific initial state preparation. We demonstrate the feasibility of super-precision measurement by utilizing the critical divergent feature of QFI. Compared with the standard Rabi model, the huge frequency ratio between the cavity and the mechanical oscillator is adjustable and easy to be implemented by only changing the frequency of the driving laser in our proposal. Due to the excellent scalability of mechanical oscillators to various physical systems, the scheme in our work could be applied to quantum sensing for measuring classical quantities and macroscopic quantum phenomena.

ACKNOWLEDGMENTS

This work was supported by the National Key Research & Development Program of China under Grant No. 2021YFA1400900, by National Natural Science

Foundation of China under Grant Nos. 12274376, 12074232, 12125406, U21A20434, 12074346, 12147149, 12204424, by the major science and technology project of Henan Province under Grant No. 221100210400, by the China Postdoctoral Science Foundation under Grant No. 2022M722889, by Natural Science Foundation of Henan Province under Grant Nos. 232300421075, 212300410085.

Appendix A: The Derivation of the QFI around Critical Point

The form of Eq. (13) can be not directly obtained, but some terms can be discarded under some conditions [10]. Since the formula of h_{ξ} has already been known, the exact QFI can be calculated as

$$I_{\xi} = 4t^{2} \operatorname{Var}[H_{1}]_{|\Psi_{0}\rangle} + h^{2}(t) \Lambda^{-2} \operatorname{Var}[C]_{|\Psi_{0}\rangle} + j^{2}(t) \Lambda^{-3} \operatorname{Var}[D]_{|\Psi_{0}\rangle} + \mathcal{C}(t),$$
(A1)

where $h(t) = 2[\sin(\sqrt{\Lambda}t) - \sqrt{\Lambda}t]$, $j(t) = 2[\cos(\sqrt{\Lambda}t) - 1]$, and the covariance term

$$C(t) = 2h(t)t\Lambda^{-1} \operatorname{Cov} [H_1, C]_{|\Psi_0\rangle} - 2j(t)t\Lambda^{-\frac{3}{2}}$$

$$\operatorname{Cov} [H_1, D]_{|\Psi_0\rangle} - h(t)j(t)\Lambda^{-\frac{5}{2}} \operatorname{Cov} [C, D]_{|\Psi_0\rangle},$$
(A2)

with the definition $\operatorname{Cov}\left[\mathcal{C}_{1},\mathcal{C}_{2}\right]_{|\Psi_{0}\rangle}=\langle\Psi_{0}\left|\mathcal{C}_{1}\mathcal{C}_{2}+\mathcal{C}_{2}\mathcal{C}_{1}\right|\Psi_{0}\rangle-2\langle\Psi_{0}\left|\mathcal{C}_{1}\right|\Psi\rangle\langle\Psi_{0}\left|\mathcal{C}_{2}\right|\Psi_{0}\rangle$. Obviously, the third term of Eq. (A1) makes the dominant contribution as $\lambda\to1$, i.e. the parameter $\xi\to\xi_{c}$. Thus, we can neglect the other low-order terms under the conditions $\sqrt{\Lambda}t=\mathcal{O}(1)$ and $\operatorname{Var}\left[D\right]\neq0$ which keep divergent scaling of I_{ξ} . The final approximate form is obtained as

$$I_{\xi} \simeq 4 \frac{\left[\sin(\sqrt{\Lambda}t) - \sqrt{\Lambda}t\right]^2}{\Lambda^3} \text{Var}\left[D\right]_{|\Psi_0\rangle}.$$
 (A3)

Appendix B: Calculations of Quadrature Dynamic Evolution of COMS

In the Heisenberg picture, the equations of motion for the quadrature operators X and P, governed by Eq. (8), are given as

$$\langle X \rangle_t = \sqrt{2} \Lambda^{-\frac{1}{2}} \sin\left(\sqrt{\Lambda}\omega_m t/2\right),$$

 $\langle P \rangle_t = \frac{\sqrt{2}}{2} \cos\left(\sqrt{\Lambda}\omega_m t/2\right),$ (B1)

from which the susceptibility with respect to λ can be obtained as

$$\partial_{\lambda}\langle X\rangle_{t} = 4\sqrt{2}\lambda\Lambda^{-3/2}\sin\left(\sqrt{\Lambda}\omega_{m}t/2\right)$$
$$-2\sqrt{2}\lambda\omega_{m}t\Lambda^{-1}\cos\left(\sqrt{\Lambda}\omega_{m}t/2\right), \qquad (B2)$$
$$\partial_{\lambda}\langle P\rangle_{t} = \sqrt{2}\lambda\omega_{m}t\Lambda^{-1/2}\sin\left(\sqrt{\Lambda}\omega_{m}t/2\right).$$

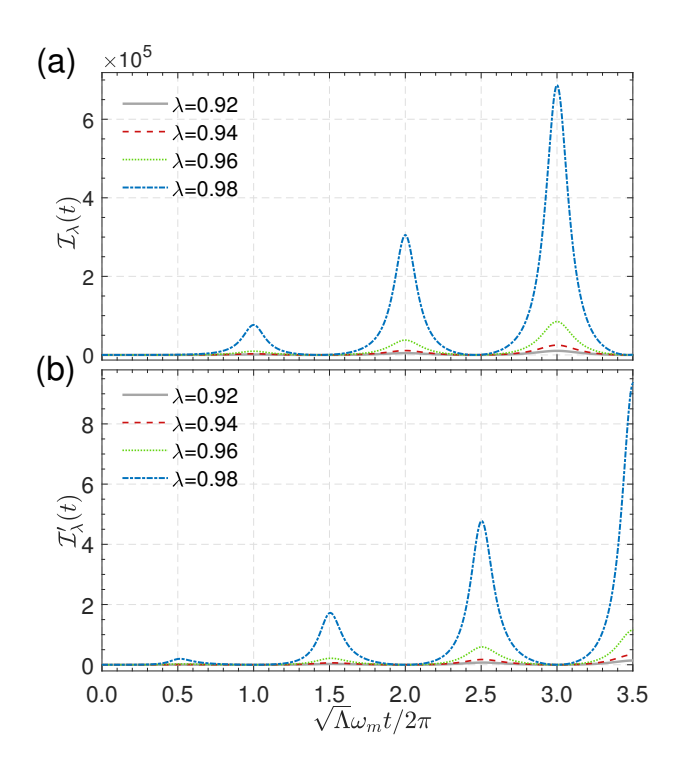


FIG. 7. The $\mathcal{I}_{\lambda}(\tau)$ and $\mathcal{I}'_{\lambda}(\tau)$ for the quadrature operators X (a) and P (b) as a function of t with the periodic peaks occurring at even periods $\tau_n = 2n\pi/(\sqrt{\Lambda}\omega_m)$ $(n \in \mathbb{Z}^+)$ for X and the odd periods $\tau_n = (2n+1)\pi/(\sqrt{\Lambda}\omega_m)$ for P, respectively. The peaks of $\mathcal{I}_{\lambda}(\tau)$ and $\mathcal{I}'_{\lambda}(\tau)$ increase with time τ_n , meaning a higher precision.

Next, we calculate the expectation of the square operator in the Heisenberg picture as

$$\begin{split} \left\langle X^{2}\right\rangle_{t} &= 1 + 2\lambda^{2}\Lambda^{-1}\left[1 - \cos\left(\sqrt{\Lambda}\omega_{m}t\right)\right],\\ \left\langle P^{2}\right\rangle_{t} &= 1 + \lambda^{2}\left[\cos\left(\sqrt{\Lambda}\omega_{m}t\right) - 1\right]/2. \end{split} \tag{B3}$$

Then, we can obtain the variance of the quadrature X and P with the formula $(\Delta O)^2 = \langle O^2 \rangle_t - \langle O \rangle_t^2$ as (O denotes an operator)

$$(\Delta X)^2 = 1 + \Lambda^{-1} \left(2\lambda^2 - 1 \right) \left[1 - \cos \left(\sqrt{\Lambda} \omega_m t \right) \right],$$

$$(\Delta P)^2 = \frac{3}{4} - \frac{\lambda^2}{2} + \left(\frac{\lambda^2}{2} - \frac{1}{4} \right) \cos \left(\sqrt{\Lambda} \omega_m t \right).$$
(B4)

According to $(\delta\lambda)^2 = (\Delta O)^2/(\partial_\lambda \langle O \rangle)^2 \geq 1/I_\lambda$ in quantum parameter estimation theory, we define $\mathcal{I}_\lambda = (\partial_\lambda \langle X \rangle_t)^2/(\Delta X)^2$ where the larger \mathcal{I}_λ is, the higher the precision is, and the closer to $I_\lambda \mathcal{I}_\lambda$ is, the closer to the limit the precision is.

Considering the quadrature X at local maximums point $t=\tau_n=2n\pi/(\sqrt{\Lambda}\omega_m)\,(n\in\mathbb{Z}^+)$, We can obtain that $\partial_\lambda\langle X\rangle_t=(-1)^{n-1}\,(2\sqrt{2})\,\lambda\omega_m\tau_n/\Lambda$ and $(\Delta X)^2=1$. Hence, $\mathcal{I}_\lambda=32\lambda^2\pi^2n^2\Lambda^{-3}$ has the same order with the QFI $I_\lambda\left(\tau_n\right)=64\lambda^2\pi^2n^2\Lambda^{-3}\mathrm{Var}\left[P^2\right]_{|\varphi\rangle_m}$, and the detailed periodic change of \mathcal{I}_λ can be witnessed from Fig. 7(a). Similarly, we can obtain the quadrature P at

the local maximums point $t = \tau'_n = (2n+1) \pi/(\sqrt{\Lambda}\omega_m)$ which is the odd multiple of $\pi/(\sqrt{\Lambda}\omega_m)$ (see Fig. 7(b)), thus showing the alternate change pattern with the time.

The figure of $\mathcal I$ can be obtained in the same way when the initial state is prepared in the coherence state. Here we will not repeat the calculation process. In brief, COMS model exhibits the same high precision at $\eta \to \infty$ compared with Rabi model. Additionally, this dynamic framework is a nice way to study mechanical cavity by bosonic field.

Appendix C: The SW Transformation of COMS with Higher-order Term

In the main text, the generator S of SW transformation has already been approximated in the condition $\eta = \Delta/\omega_m \gg 1$. Here, we will reach a more precise generator \tilde{S} which holds for the finite frequency ratio [27, 48, 49]. The Hamiltonian H_L satisfies the form of $H_s - GV$, with $H_s = \Delta a^{\dagger} a + \omega_m b^{\dagger} b$ and $V = (a^{\dagger} + a)(b^{\dagger} + b)$. Next, considering a unitary transformation $\tilde{U} = e^{\tilde{S}}$, the transformed Hamiltonian can be written as

$$\tilde{H}_L = e^{-\tilde{S}} H_L e^{\tilde{S}} = \sum_{k=0}^{\infty} \frac{1}{k!} \left[H_L^{(k)}, \tilde{S} \right].$$
 (C1)

Divide the transformed Hamiltonian into the diagonal part $\tilde{H}_{\rm d}$ and off-diagonal part $\tilde{H}_{\rm od}$ by defining \tilde{S} as block-off-diagonal and using the fact that V is block-diagonal, which can be obtained as

$$\tilde{H}_{d} = \sum_{k=0}^{\infty} \frac{\left[H_{s}^{(2k)}, \tilde{S}\right]}{2k!} - \sum_{k=0}^{\infty} \frac{\left[GV^{(2k+1)}, \tilde{S}\right]}{(2k+1)!},$$

$$\tilde{H}_{od} = \sum_{k=0}^{\infty} \frac{\left[H_{s}^{(2k+1)}, \tilde{S}\right]}{(2k+1)!} - \sum_{k=0}^{\infty} \frac{\left[GV^{(2k)}, \tilde{S}\right]}{(2k)!}.$$
(C2)

Now, we can give the generator \hat{S} as

$$\tilde{S} = G\tilde{S}_1 + G^3\tilde{S}_3 \tag{C3}$$

by keeping to the third order in G. \tilde{S}_1 and \tilde{S}_3 can be calculated by the formula

$$\begin{bmatrix} H_s, \tilde{S}_1 \end{bmatrix} = V,
\begin{bmatrix} H_s, \tilde{S}_3 \end{bmatrix} = \frac{1}{3} \left[\left[V, \tilde{S}_1 \right], \tilde{S}_1 \right].$$
(C4)

We find that the generator \tilde{S} satisfies the conditions in Eq. (C4) as

$$\tilde{S}_{1} = \frac{1}{\Delta} (b + b^{\dagger}) (a^{\dagger} - a) + \frac{\omega_{m}}{\Delta^{2}} (b - b^{\dagger}) (a + a^{\dagger})
+ \mathcal{O} \left(\frac{\omega_{m}}{\Delta^{3}}\right),
\tilde{S}_{3} = \frac{2}{3\Delta^{3}} \left[(b + b^{\dagger})^{3} - (b - b^{\dagger})^{2} - (b + b^{\dagger}) \right] (a + a^{\dagger})
+ \frac{2\omega_{m}}{3\Delta^{4}} \left[(a + a^{\dagger})^{3} - (a - a^{\dagger})^{2} - (a + a^{\dagger}) \right] (b + b^{\dagger})
+ \mathcal{O} \left(\frac{\omega_{m}}{\Delta^{4}}\right).$$
(C5)

Next, we can use Eq. (C3) to rearrange the generator \tilde{S}

$$\tilde{S} = \frac{\lambda}{2} \eta^{-\frac{1}{2}} (b + b^{\dagger}) (a^{\dagger} - a) + \frac{\lambda}{2} \eta^{-\frac{3}{2}} (b - b^{\dagger}) (a + a^{\dagger})$$

$$+ \frac{\lambda^{3}}{12} \eta^{-\frac{3}{2}} \left[(b + b^{\dagger})^{3} - (b - b^{\dagger})^{2} - (b + b^{\dagger}) \right] (a + a^{\dagger})$$

$$+ \mathcal{O} \left(\lambda^{3} \eta^{-\frac{5}{2}} \right),$$
(C6)

where $\lambda = 2G/\sqrt{\Delta\omega_m}$ and $\eta = \Delta/\omega_m$. Inserting the generator \tilde{S} into the Hamiltonian, we can reach

$$\tilde{H}_{L} = \Delta a^{\dagger} a + \omega_{m} b^{\dagger} b - \frac{\lambda^{2}}{4} \omega_{m} \left(b^{\dagger} + b \right)^{2}$$

$$- \frac{\lambda^{2}}{4} \eta^{-1} \omega_{m} \left(a^{\dagger} + a \right)^{2} - \frac{1}{24} \lambda^{4} \eta^{-2} \omega_{m}$$

$$\left(b^{\dagger} + b \right)^{2} + \mathcal{O} \left(\lambda^{4} \eta^{-3} \right).$$
(C7)

In the main text, Eq. (8) only takes the first three terms for $\eta \gg 1$. When we consider the effect of finite frequency ratio of COMS, we cannot be neglect higher-order terms.

- V. Giovannetti, S. Lloyd, and L. Maccone, Science 306, 1330 (2004).
- [2] V. Giovannetti, S. Lloyd, and L. Maccone, Nature Photonics 5, 222 (2011).
- [3] C. L. Degen, F. Reinhard, and P. Cappellaro, Reviews of Modern Physics 89, 035002 (2017).
- [4] V. Giovannetti, S. Lloyd, and L. Maccone, Physical Review Letters 96, 010401 (2006).
- [5] S. Sachdev, Quantum Phase Transitions, 2nd ed. (Cambridge Univ. Press, Cambridge, 2013).
- [6] M. M. Rams, P. Sierant, O. Dutta, P. Horodecki, and J. Zakrzewski, Physical Review X 8, 021022 (2018).
- [7] I. Frérot and T. Roscilde, Physical Review Letters 121, 020402 (2018).
- [8] L. Li and J.-Q. Zhang, Photonics 8, 588 (2021).
- [9] K. Macieszczak, M. Gută, I. Lesanovsky, and J. P. Garrahan, Physical Review A 93, 022103 (2016).
- [10] Y. Chu, S. Zhang, B. Yu, and J. Cai, Physical Review Letters 126, 010502 (2021).
- [11] J.-H. Lü, W. Ning, X. Zhu, F. Wu, L.-T. Shen, Z.-B. Yang, and S.-B. Zheng, Physical Review A 106, 062616 (2022).
- [12] M. W. Mitchell, J. S. Lundeen, and A. M. Steinberg, Nature 429, 161 (2004).
- [13] P. Walther, J.-W. Pan, M. Aspelmeyer, R. Ursin, S. Gasparoni, and A. Zeilinger, Nature 429, 158 (2004).
- [14] A. Luis, Physical Review A **64**, 054102 (2001).
- [15] J. Joo, W. J. Munro, and T. P. Spiller, Physical Review Letters 107, 083601 (2011).
- [16] W. van Dam, G. M. D'Ariano, A. Ekert, C. Macchiavello, and M. Mosca, Physical Review Letters 98, 090501 (2007).
- [17] L. Maccone and G. De Cillis, Physical Review A 79, 023812 (2009).
- [18] B. Yurke, S. L. McCall, and J. R. Klauder, Physical Review A 33, 4033 (1986).

- [19] T. Kim, O. Pfister, M. J. Holland, J. Noh, and J. L. Hall, Physical Review A 57, 4004 (1998).
- [20] R. H. Dicke, Physical Review 93, 99 (1954).
- [21] L. Bakemeier, A. Alvermann, and H. Fehske, Physical Review A 85, 043821 (2012).
- [22] L. Garbe, I. L. Egusquiza, E. Solano, C. Ciuti, T. Coudreau, P. Milman, and S. Felicetti, Physical Review A 95, 053854 (2017).
- [23] M. Liu, S. Chesi, Z.-J. Ying, X. Chen, H.-G. Luo, and H.-Q. Lin, Physical Review Letters 119, 220601 (2017).
- [24] X.-Y. Chen and Y.-Y. Zhang, Physical Review A 97, 053821 (2018).
- [25] I. I. Rabi, Physical Review **51**, 652 (1937).
- [26] S. Ashhab, Physical Review A 87, 013826 (2013).
- [27] M.-J. Hwang, R. Puebla, and M. B. Plenio, Physical Review Letters 115, 180404 (2015).
- [28] F. Marquardt and S. Girvin, Physics 2, 40 (2009).
- [29] E. Verhagen, S. Deléglise, S. Weis, A. Schliesser, and T. J. Kippenberg, Nature 482, 63 (2012).
- [30] W. P. Bowen, *Quantum Optomechanics*, zeroth ed. (CRC Press, 2015).
- [31] J.-Q. Zhang, Y. Li, M. Feng, and Y. Xu, Physical Review A 86, 053806 (2012).
- [32] H. Xiong, L.-G. Si, X. Yang, and Y. Wu, Applied Physics Letters **107**, 091116 (2015).
- [33] S. B. Jäger, J. Cooper, M. J. Holland, and G. Morigi, Physical Review Letters 123, 053601 (2019).
- [34] Z. Wang, J. Lian, J.-Q. Liang, Y. Yu, and W.-M. Liu, Physical Review A 93, 033630 (2016).
- [35] J.-Q. Liao, J.-F. Huang, and L. Tian, Physical Review A 93, 033853 (2016).
- [36] U. B. Hoff, J. Kollath-Bönig, J. S. Neergaard-Nielsen, and U. L. Andersen, Physical Review Letters 117, 143601 (2016).
- [37] K. Jähne, C. Genes, K. Hammerer, M. Wallquist, E. S. Polzik, and P. Zoller, Physical Review A 79, 063819 (2009).

- [38] R. A. Fisher, Mathematical Proceedings of the Cambridge Philosophical Society 22, 700 (1925).
- [39] S. L. Braunstein and C. M. Caves, Physical Review Letters 72, 3439 (1994).
- [40] J. Liu, X.-X. Jing, W. Zhong, and X.-G. Wang, Communications in Theoretical Physics **61**, 45 (2014).
- [41] S. Barzanjeh, A. Xuereb, S. Gröblacher, M. Paternostro, C. A. Regal, and E. M. Weig, Nature Physics 18, 15 (2022).
- [42] M. Sansa, M. Defoort, A. Brenac, M. Hermouet, L. Banniard, A. Fafin, M. Gely, C. Masselon, I. Favero, G. Jourdan, and S. Hentz, Nature Communications 11, 3781 (2020).
- [43] H. Xiong, Z.-X. Liu, and Y. Wu, Optics Letters **42**, 3630
- [44] J. Chan, T. P. M. Alegre, A. H. Safavi-Naeini, J. T. Hill, A. Krause, S. Gröblacher, M. Aspelmeyer, and O. Painter, Nature 478, 89 (2011).
- [45] F. Fogliano, B. Besga, A. Reigue, P. Heringlake, L. Mercier de Lépinay, C. Vaneph, J. Reichel, B. Pigeau, and O. Arcizet, Physical Review X 11, 021009 (2021).
- [46] D.-Y. Wang, C.-H. Bai, H.-F. Wang, A.-D. Zhu, and S. Zhang, Scientific Reports 6, 24421 (2016).
- [47] D.-Y. Wang, C.-H. Bai, H.-F. Wang, A.-D. Zhu, and S. Zhang, Scientific Reports 6, 38559 (2016).
- [48] J. R. Schrieffer and P. A. Wolff, Physical Review 149, 491 (1966).
- [49] S. Bravyi, D. P. DiVincenzo, and D. Loss, Annals of Physics 326, 2793 (2011).
- [50] S. Pang and A. N. Jordan, Nature Communications 8, 14695 (2017).
- [51] S. Pang and T. A. Brun, Physical Review A 90, 022117 (2014).

- [52] R. M. Wilcox, Journal of Mathematical Physics 8, 962 (1967).
- [53] J. D. Teufel, T. Donner, D. Li, J. W. Harlow, M. S. Allman, K. Cicak, A. J. Sirois, J. D. Whittaker, K. W. Lehnert, and R. W. Simmonds, Nature 475, 359 (2011).
- [54] C. Genes, D. Vitali, P. Tombesi, S. Gigan, and M. Aspelmeyer, Physical Review A 77, 033804 (2008).
- [55] O. Arcizet, P.-F. Cohadon, T. Briant, M. Pinard, and A. Heidmann, Nature 444, 71 (2006).
- [56] R. W. Peterson, T. P. Purdy, N. S. Kampel, R. W. Andrews, P.-L. Yu, K. W. Lehnert, and C. A. Regal, Physical Review Letters 116, 063601 (2016).
- [57] J. D. Teufel, F. Lecocq, and R. W. Simmonds, Physical Review Letters 116, 013602 (2016).
- [58] J. Alonso, F. M. Leupold, Z. U. Solèr, M. Fadel, M. Marinelli, B. C. Keitch, V. Negnevitsky, and J. P. Home, Nature Communications 7, 11243 (2016).
- [59] K. C. McCormick, J. Keller, S. C. Burd, D. J. Wineland, A. C. Wilson, and D. Leibfried, Nature 572, 86 (2019).
- [60] N. E. Frattini, R. G. Cortiñas, J. Venkatraman, X. Xiao, Q. Su, C. U. Lei, B. J. Chapman, V. R. Joshi, S. M. Girvin, R. J. Schoelkopf, S. Puri, and M. H. Devoret, (2022), 10.48550/ARXIV.2209.03934.
- [61] M. Abdi, P. Degenfeld-Schonburg, M. Sameti, C. Navarrete-Benlloch, and M. J. Hartmann, Physical Review Letters 116, 233604 (2016).
- [62] J.-Q. Liao and L. Tian, Physical Review Letters 116, 163602 (2016).
- [63] H. Xie, X. Shang, C.-G. Liao, Z.-H. Chen, and X.-M. Lin, Physical Review A 100, 033803 (2019).